s-wave Helium

A new approach

Abstract

The s-wave Helium model is used to examplify a cycle expansion of the Zeta function. Cycles (up to code length 6) are found using 'two parameter search', a method described in [1]. Zeros for the Zeta function are found using simple numerical methods. The resulting energy spectrum is compared to a spectrum based on the same cycle expansion, calculated by M. Draeger and collaborators [2], and another spectrum from the same paper based on quantum mechanical calculations. Finally, a tempting problem that has not yet been solved is presented.

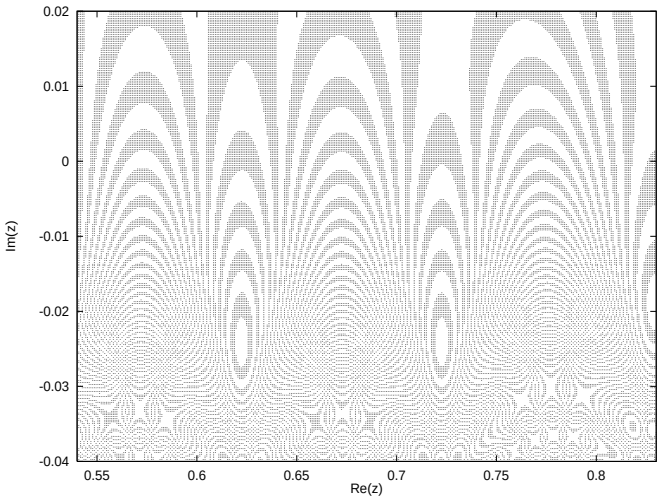

s-wave Helium

A new approach

An exam project for the course on

Classical and Quantum Chaos, spring 1995

Started June 25, 1995

Finished ~~August 11, 1995~~

Author: Kristian Schaadt

Supervisor: Predrag Cvitanović

1 The s-wave model

The s-wave model was introduced by G. Handke, M. Draeger and H. Friedrich [2] as an approximation to the full Helium problem. As will appear in the following, the model represents a quite crude approximation, but the resulting energy spectrum comes surprisingly close to the real spectrum. We present here a new approach to the integration of the equations of motion, applying a coordinate transformation originally used by G. Tanner and D. Wintgen for the colinear Helium model. We shall return to this essential point in the discussion of the results obtained by our method compared to the results in [6].

1.1 The Hamiltonian in usual coordinates

Classically, the Hamiltonian for a system consisting of three charged particles is given by

$$\tilde{H} = \sum_{i=1}^{3} \frac{\tilde{\mathbf{p}}_i^2}{2m_i} + Z_1 Z_2 \frac{e^2}{\tilde{r}_{12}} + Z_1 Z_3 \frac{e^2}{\tilde{r}_{13}} + Z_2 Z_3 \frac{e^2}{\tilde{r}_{23}} \tag{1}$$

Here, $\tilde{r}_{ij} = \mid \tilde{\mathbf{q}}_i - \tilde{\mathbf{q}}_j \mid$, the $\tilde{\mathbf{q}}_i$'s being the coordinates in three dimensions, and the $\tilde{\mathbf{p}}_i$'s the corresponding momenta. The classical Helium atom corresponds to $Z_1 = Z_2 = -1$, $Z_3 = 2$.

It is possible [5] to scale the energy, i.e. from solving the equations of motion for the scaled Hamiltonian

$$H' = \sum_{i=1}^{3} \frac{\mathbf{p'}_i^2}{2m_i} + Z_1 Z_2 \frac{1}{r'_{12}} + Z_1 Z_3 \frac{1}{r'_{13}} + Z_2 Z_3 \frac{1}{r'_{23}} \tag{2}$$

we get a solution of (1) for an energy E by the scaling transformation

$$\tilde{r}_{ij} = \frac{e^2}{(\pm E)} r'_{ij} \qquad \tilde{\mathbf{p}}_i = \sqrt{\pm E}\, \mathbf{p}'_i \qquad \tilde{t} = \frac{e^2}{(\pm E)^{3/2}} t' \qquad \tilde{S} = \frac{e^2}{(\pm E)^{1/2}} S' \tag{3}$$

We now assume that the nucleus is immobile, i.e. $m_3 = \infty$. Furthermore, we make at this point the assumption of the s-wave model: Both electrons are restricted to spherical states with individual angular momentum zero. This corresponds to the classical assumption that the electrons are each just a spherical shell of uniformly distributed charge -e, with the nuclear charge of +2e placed in the mutual center of the spheres. The hamiltonian (2) now becomes

$$H = \frac{p_1^2}{2} + \frac{p_2^2}{2} - \frac{Z}{r_<} - \frac{Z-1}{r_>} \tag{4}$$

In this equation, Z is the nuclear charge, $r_<$ is the smaller of the to radii, $r_>$ the greater. The equation reflects the fact that the inner electron feels the whole nuclear charge Z, while the outer only feels a charge of $Z-1$, since it is 'screened' by the inner electron.

Due to the scaling transformation (3) we only have to consider $H = E = \pm 1$. A periodic orbit is a bound state with negative energy for both electrons and consequently negative total energy. In the task of looking for cycles we therefore consider $H = E = -1$.

1.2 Transformation of coordinates

Looking for cycles, one way to go is to perform numerical integration of the equations of motion. However, H contains three singularities: $r_1 = 0$, $r_2 = 0$ and $r_1 = r_2 = 0$, where r_1 and r_2 are the radii of the two electrons. The first two can be overcome by the Kustaanheimo-Stiefel transformation of coordinates, as presented below. The third one is an essential singularity of Hamiltons equations, i.e. the equations of motion can not be uniquely continued through this third singularity, and consequently, it can not be overcome by any transformation of coordinates. In order to use the Kustaanheimo-Stiefel transformation we consider the two cases $r_1 < r_2$ and $r_1 > r_2$ for the Hamiltonian (4):

$$H = \frac{p_1^2}{2} + \frac{p_2^2}{2} - \frac{Z}{r_1} - \frac{Z-1}{r_2} \qquad r_1 < r_2 \tag{5}$$

$$H = \frac{p_1^2}{2} + \frac{p_2^2}{2} - \frac{Z}{r_2} - \frac{Z-1}{r_1} \qquad r_1 > r_2 \tag{6}$$

We introduce now the coordinates Q_1, Q_2, P_1 and P_2 through

$$r_1 = Q_1^2 \qquad p_1 = \frac{P_1}{2Q_1} \tag{7}$$

$$r_2 = Q_2^2 \qquad p_2 = \frac{-P_2}{2Q_2} \tag{8}$$

along with a new time parametrization, introduced through

$$d\tau = \frac{dt}{r_1 r_2} \tag{9}$$

Using the following Hamiltonian with the new time τ, the Hamiltonian structure is conserved (we have not checked this, but a proof is given in [3]).

$$\begin{aligned} H_r = &\ \tfrac{1}{8}(P_1^2 Q_2^2 + P_2^2 Q_1^2) - Z Q_2^2 - (Z-1)Q_1^2 + Q_1^2 Q_2^2 \qquad Q_1^2 < Q_2^2 \\ H_r = &\ \tfrac{1}{8}(P_1^2 Q_2^2 + P_2^2 Q_1^2) - Z Q_1^2 - (Z-1)Q_2^2 + Q_1^2 Q_2^2 \qquad Q_1^2 > Q_2^2 \end{aligned} \tag{10}$$

Considering bound motion i.e. $H = -1$ now corresponds to considering $H_r = 0$. The Hamiltonian equations of motion for $Q_1^2 < Q_2^2$ now reads:

$$\begin{aligned} \dot{P}_1 = -\frac{\partial H_r}{\partial Q_1} = &\ 2Q_1(Z - 1 - \tfrac{1}{8}P_2^2 - Q_2^2) \qquad \dot{Q}_1 = \frac{\partial H_r}{\partial P_1} = \frac{1}{4}Q_2^2 P_1 \\ \dot{P}_2 = -\frac{\partial H_r}{\partial Q_2} = &\ 2Q_1(Z - \tfrac{1}{8}P_1^2 - Q_1^2) \qquad \dot{Q}_2 = \frac{\partial H_r}{\partial P_2} = \frac{1}{4}Q_1^2 P_2 \end{aligned}$$

And for $Q_1^2 > Q_2^2$:

$$\dot{P}_1 = -\frac{\partial H_r}{\partial Q_1} = \quad 2Q_1(Z - \tfrac{1}{8}P_2^2 - Q_2^2) \qquad \dot{Q}_1 = \frac{\partial H_r}{\partial P_1} = \frac{1}{4}Q_2^2 P_1$$
$$\dot{P}_2 = -\frac{\partial H_r}{\partial Q_2} = \quad 2Q_1(Z - 1 - \tfrac{1}{8}P_1^2 - Q_1^2) \qquad \dot{Q}_2 = \frac{\partial H_r}{\partial P_2} = \frac{1}{4}Q_1^2 P_2$$

This is not the form used in original articles, but our application of methods oused by Wintgen and Tanner [5] to the Hamiltonian (4). Using these equations and fourth order Runge-Kutta integration, we have computed trajectories for the s-wave Helium system.

2 Looking for cycles

The periodic orbits of a system with well-ordered symbolic dynamics can be found using 'two parameter search'. This method is described in [1]. Before we can give a summery of its application to s-wave Helium, we must introduce symbolic dynamics, by considering what happens to points in the Poincaré plane as the system evolves.

2.1 Symbolic dynamics

The flow takes place in (Q_1,Q_2,P_1,P_2)-space. We choose a Poincaré section $Q_2^2 = 0$. From (10) and $H_r = 0$ one can find P_2, given Q_1^2, so the Poincaré plane is the (Q_1^2,P_1)-plane. We can now start out at any point in this plane, integrating the flow as described above. A good way to keep track of the trajectories is to write down the string $s_1 s_2 s_3 ...$ of symbols defined by saying that s_n corresponds to the n'th collision between an electron and the nucleus, and s_n is given by

$$s_n = \begin{cases} 0 & \text{if last collision was with same electron} \\ 1 & \text{if last collision was with other electron} \end{cases} \tag{11}$$

Let us consider now the iterative process of writing down this symbol string. Starting out at a point in the Poincaré plane, we can tell the computer to go just one iteration forward, assigning one color if the next symbol is a '0' and a different color if it is a '1'. Doing this for a large number of points the Poincaré plane will produce two different-colored areas. Going on in the same manner will produce 2^n areas after n iterations. We can think of the areas as labeled with symbol strings of length n. After infinitely many iterations, all symbol sequences are represented, i.e we are dealing with complete Smale Horseshoe dynamics, and some part of the Poincaré plane has been divided into infinitely thin strips, ordered as a binary Cantor set. That we are dealing with a complete Smale Horseshoe is not trivial and no proof exists, but it seems to be a fact that different

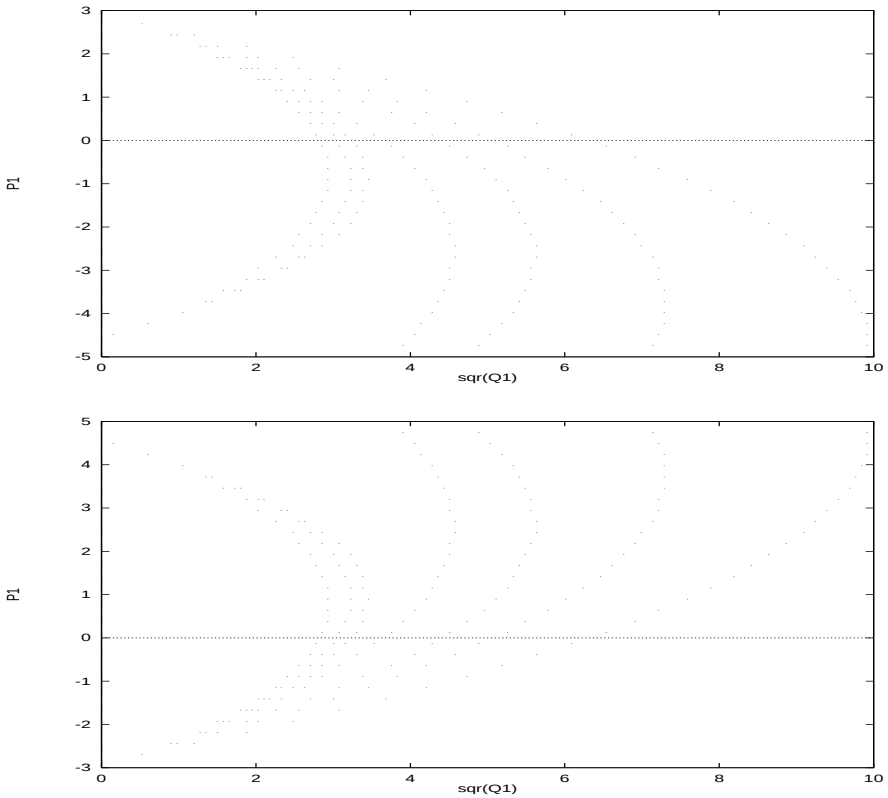

Figure 1: Upper picture: The division of the Poincaré plane into 2^n thin strips after n iterations illustrated here for $n = 3$. Lower picture: Same as upper picture, but for integration backwards in time. Integration backwards in time is done by shifting the signs of the momenta. If we shift at the same time the signs of Q_2 and P_2 (it is obvious from the equations of motion that this does not change the flow), we have all in all only shifted the sign of P_1. But for the Poincaré plane this is just a reflection through the Q_1^2-axis. Both pictures: Intersection of the forward and backward partitioning of the Poincaré plane yields the Smale horseshoe.

authers agree about [1,2]. The best way to convince oneself about its validity is to look at iterations of the Poincaré plane forward and backward in time, and check that all of the forward strings intersect all of the backward strings as illustrated in figure 1. To illustrate that this is a special case, we mention that at lower nuclear charge, one does no longer have a complete Smale horseshoe and some symbol sequences will not be realised, i.e. they are 'pruned' away [4].

The very special sequences that are just repetitions of a finite symbol string represent s-wave Helium periodic orbits, and they appear in the Poincaré plane as isolated points. As an example, consider the finite symbol string '010111'. This string represents a cycle. The string '101011', of course, represents the same cycle, but it is not represented by the same point in the Poincaré space. If a cycle is represented by a symbol string

of length m, it will therefore be represented by m different points in the Poincaré plane, corresponding to the m different ways to write down this string.

An illustration of the partition of the Poincaré plane can be seen in figure 1. Here, however, another coding has been used, yielding *well ordered* symbolic dynamics. This will be explained in the following. The coding used to obtain figure 1 is simply

$$w_n = \begin{cases} 0 & \text{if the collision is with electron 1} \\ 1 & \text{if the collision is with electron 2} \end{cases} \tag{12}$$

The rightmost strip consists of the points in the Poincaré plane that by forward integration produce the symbol string '111', using the coding explained above. Moving from right to left, this coding gives for the eight strips:'111', '110', '101', '100', '011', '010', '001', '000'. As one can see, this is an example of well ordered dynamics.

The well ordered symbolic string w_n can also be obtained from the s_n-string by setting $w_1{=}s_1$ and then

$$w_{n+1} = \begin{cases} w_n & \text{if } s_{n+1} = 0 \\ 1 - w_n & \text{if } s_{n+1} = 1 \end{cases} \tag{13}$$

Let us start out from a point S in the Poincaré plane. We now define the *symbolic future* $\gamma(S)$ for this point to be

$$\gamma(S) = 0.w_1 w_2 w_3 ... = \sum_{n=1}^{\infty} \frac{w_n}{2^n} \tag{14}$$

where we have used the symbol string w_n representing the future trajectory, defined above. Similarily, we can again start out at the point S, but let the flow go backwards in time, defining the *symbolic past* $\delta(S)$ as $w_0 = s_0$ and then

$$w_{n-1} = \begin{cases} w_n & \text{if } s_{n-1} = 0 \\ 1 - w_n & \text{if } s_{n-1} = 1 \end{cases} \tag{15}$$

$$\delta(S) = 0.w_0 w_{-1} w_{-2} ... = \sum_{n=1}^{\infty} \frac{w_{1-n}}{2^n} \tag{16}$$

The actual computation of the symbolic past is done by simply reversing the momentum for both electrons and then performing numerical integration as usual. Let us return now to the subject of well ordered symbolic dynamics, since this is essential for understanding the two parameter search. We consider still the Poincaré plane. Starting at the P_1-axis and moving in the direction of increasing Q_1^2, parallel to the Q_1^2-axis, one will pass by the strips mentioned before in 'natural' order, i.e. $\delta(S)$ will be monotone. It would have been nice if the same was true for $\gamma(S)$ when moving parallel to the P_1-axis, but as can be easily detected from figure 1, this is not the case, and it is not even possible to find a cartesian coordinate system where $\gamma(S)$ is monotone along one of the axes. Some elaboration on this issue can be found in the following section.

2.2 Two parameter search

It will be described first how this cycle-finding method works and then explained afterwards why it actually does find the cycles, using the facts from the preceding section.

Let us first of all clearify precisely what is the problem that two parameter search is meant to solve. We want to find cycles for s-wave Helium. Knowing from the preceding section that a cycle is labeled by a finite symbol string, we set out to find the cycle with the particular symbol string c_n, the coding in this string being as in (11). As explained in the previous section, a cycle string is represented by only one point in the Poincaré plane. One can sum up the two parameter search procedure by saying that if we input a starting point in the Poincaré plane, the procedure is supposed to guide us from this point to the unique point representing the cycle symbol string. In more detail, the procedure is as follows:

We calculate the symbolic future γ_c and the symbolic past δ_c for the cycle, converting first the c_n-string to the w_n-string by (13) and (15), and then using (14) and (16). Then we give a starting guess, defining a rectangle in the Poincaré plane by its lower left corner $(Q^2_{1,min}, P_{1,min})$ and upper right corner $(Q^2_{1,max}, P_{1,max})$. The center $(Q^2_{1,m}, P_{1,m})$ of this rectangle is given by

$$(Q^2_{1,m}, P_{1,m}) = \left(\frac{Q^2_{1,min} + Q^2_{1,max}}{2} \, , \, \frac{P_{1,min} + P_{1,max}}{2} \right) \qquad (17)$$

The rectangle in the Poincaré plane corresponds to some strange figure in the (δ, γ)-plane. However, we shall pretend it is a parallelogram. Let us assume for a moment that this parallelogram contains the point (δ_c, γ_c). In that case, if we partition the rectangle into four equally sized rectangles by cutting along the axis, through the center, then one of the four corresponding parallelograms will (probably) contain the point (δ_c, γ_c) in the (δ, γ)-plane. By comparing (δ, γ) for the center to (δ_c, γ_c), one can determine which one it is. Sometimes, however, the parallelogram chosen does not contain (δ_c, γ_c), and it will be necessary to make small corrections. Also, if the point (δ_c, γ_c) was not in the original rectangle in the first place, corrections are necessary. These corrections are introduced by enlarging the rectangle by a (small) fraction of its present size, until its corresponding parallelogram contains the point (δ_c, γ_c).

In any case, corner points for a new rectangle are found and this rectangle is then partitioned just like the original one. This iterative process is continued until the rectangle in the Poincaré plane has shrunk to the desired size, i.e. until the unique point in the Poincaré plane representing the cycle symbol string c_n is determined to within some small error. An illustration of the convergence process is shown in figure 2.

Let us now turn to the explanation of why this procedure leeds to the correct results. It is obvious that in the iterative process described above, choosing at least sometimes the correct fourth of the rectangle, is crucial.

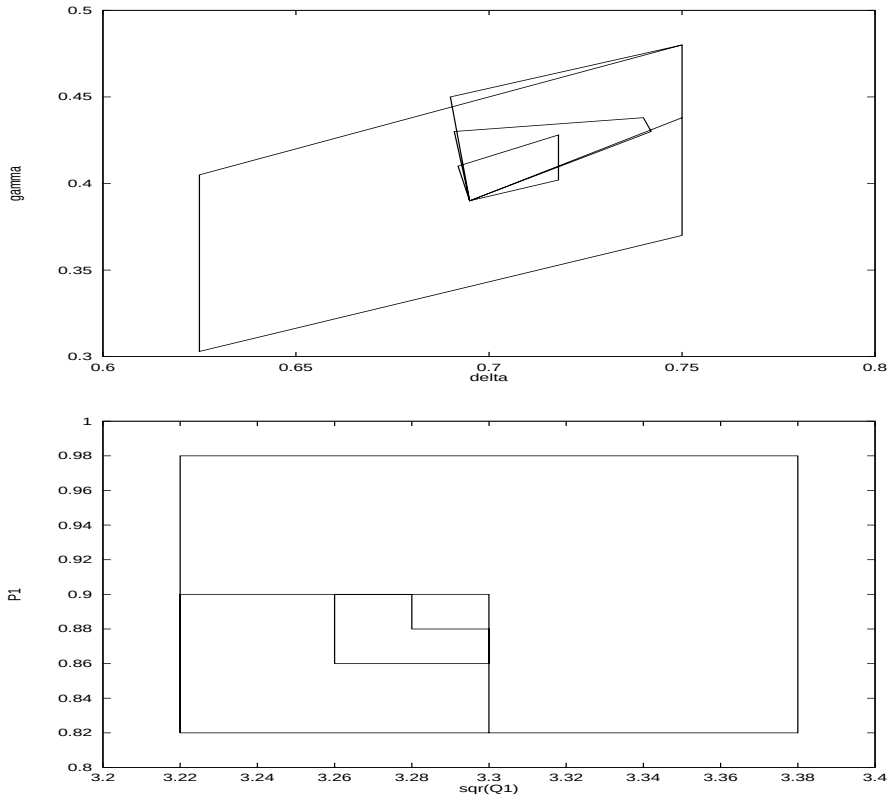

Figure 2: This is an illustration of the partitioning of the rectangles in the Poincaré plane. Boxes defined by straight lines connecting the corner points are used to visualize the unknown figures in the (δ, γ)-plane that correspond to the rectangles. The convergence shown here is idealized for the sake of clear demonstration; a normal detection of a cycle would include corrections in almost every iteration step.

This can only happen if there is a meaning to comparing (δ, γ) for the center to (δ_c, γ_c). In other words, we need δ and γ to vary monotonically along the Q_1^2-axis and the P_1-axis, correspondingly, but as we saw in the preceding section, this is not the case. We saw that γ does not vary monotonically along the P_1-axis.

Surprisingly, this problem seems to have very little effect on the convergence, even for very bad starting guesses. The explanation is probably that γ does vary monotonically with P_1 in large parts of the Poincaré plane, and certainly close to points representing cycles. In this sense, the two parameter search is an effective method for cycle determination. Other methods, such as Newton iteration of the Poincaré map, are faster but require very good starting guesses for cycles with long symbol strings. A combination of the two methods would be the best way to use them, but we have not implemented this here.

2.3 Cycle trajectories

Having described the method by which we have located the s-wave Helium cycles up to code length 6, it is about time to see what they 'look like'. A good way to get an idea of how the electrons move, is to look at the projection of the trajectory in the full phase space onto the (Q_1^2, Q_2^2)-plane. Such a projection can be seen for 6 cycles in figure 3.

3 Essential properties of the cycles

Having found the cycles we need, we determine some essential properties of each cycle in order to apply the Gutzwiller Zeta function in the next section. We consider how to calculate the action and Luapunov exponent for a cycle. The Monodromy matrix is introduced.

3.1 The action

Denoting the period for a cycle p by T_p and the action by S_p, we have [5] the relation $T_p = \frac{1}{2} S_p$. From (9), we then get

$$S_p = \frac{1}{2} T_p = \frac{1}{2} \oint dt = \frac{1}{2} \oint Q_1^2 Q_2^2 d\tau$$

where the integral is over the cycle. From this equation we determine the action for each cycle, using fourth order Runge-Kutta integration.

3.2 Lyapunov exponent

It is well known that for a multi dimensional map, the Lyapunov exponents for a fixpoint of the map are determined by the eigenvalues of the Jacobian. For a flow, when a Poincaré surface of section is defined, a periodic orbit

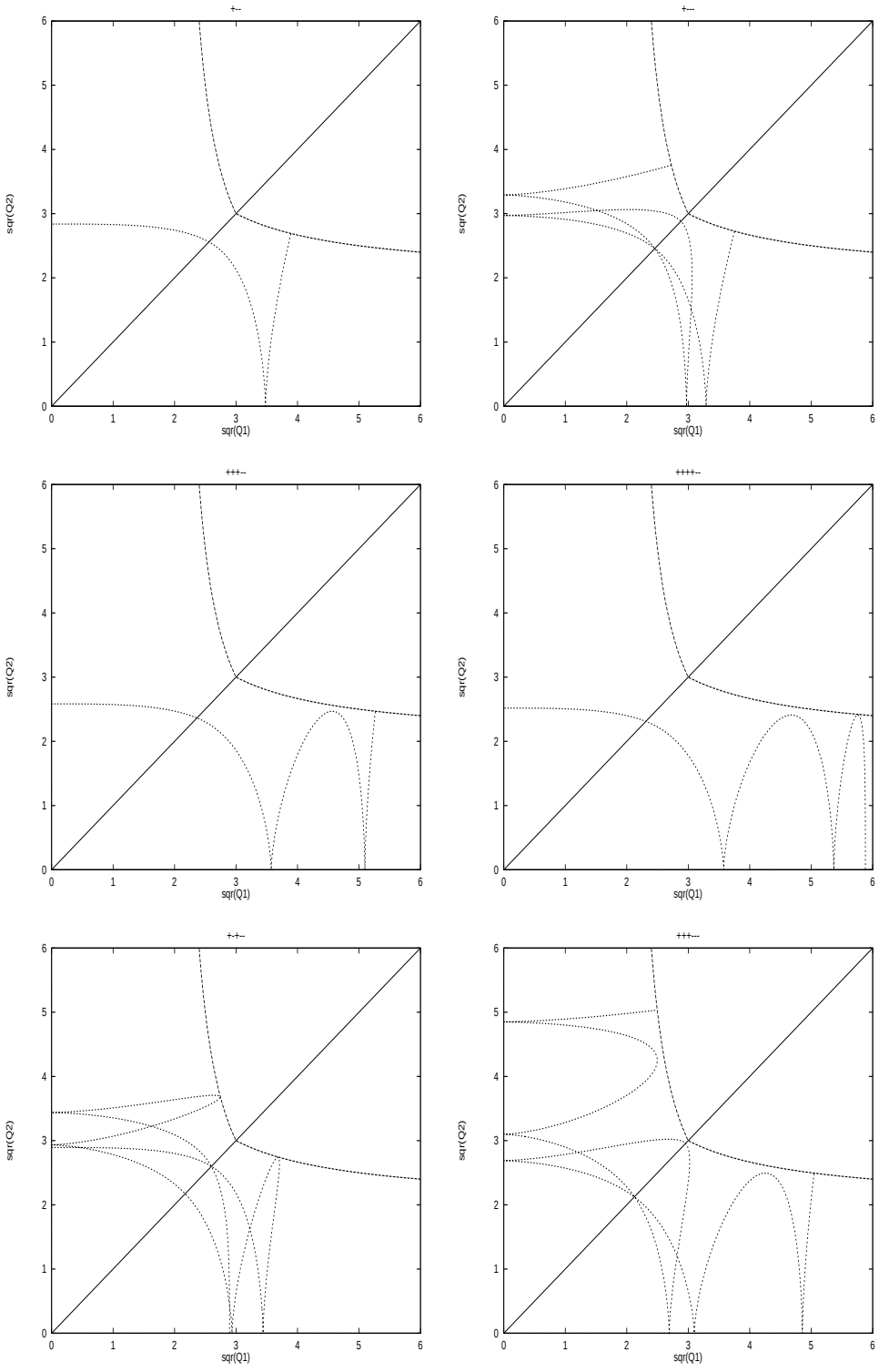

Figure 3: Projection of trajectories for 6 s-wave Helium cycles. We also show the diagonal and the equipotential line. The $(+,-)$-coding used here and on the front page is the not-well-ordered coding introduced earlier, writing '+' instead of '0' and '−' instead of '1'.

of the flow corresponds to a fixpoint of some power of the Poincaré map. In that situation one is interested in determining the 'map-Jacobian' from the 'flow-Jacobian'. This is done by integrating the 'flow-Jacobian' along the cycle. This is what we shall do in the following. The treatment will stay close to [5].
We write the Hamiltonian equations of motion as

$$\dot{x} = \omega \frac{\partial H}{\partial x} , \qquad \text{with} \quad \omega = \begin{pmatrix} 0 & \mathbf{I} \\ -\mathbf{I} & 0 \end{pmatrix}$$

where x denotes the phase space vector $x = (Q_1, Q_2, P_1, P_2)$. and $\mathbf{I}$ is the 2×2 unit matrix.
Close to a phase space trajectory $x(t) = (Q_1(t), Q_2(t), P_1(t), P_2(t))$, the linearized motion is controlled by the Jacobian and given by

$$\delta x(t) = \mathbf{J}(t) \delta x(0) \tag{18}$$

The equations of motion of $\mathbf{J}$ are given by

$$\dot{\mathbf{J}}(t) = \mathbf{L}(t)\mathbf{J}(t) \qquad \text{with} \quad \mathbf{L}(t)_{ij} = \omega \left. \frac{\partial^2 H}{\partial x_i \partial x_j} \right|_{x(t)} \tag{19}$$

It is not necessary to integrate the entire Jacobian. We can reduce the problem somewhat by choosing a suitable local coordinate system, such that the Jacobian consists of an interesting part and a trivial part. The interesting part is called the Monodromy matrix. To integrate this matrix, we need an equation of motion. The derivation of this is presented the following. First, let us explain why this is possible. At any point in phase space the flow and the gradient of the energy are perpendicular. This must be true, since the energy is constant in the direction of the flow (we are dealing with a Hamiltonian that has no explicit time dependence). An initial displacement in the direction of the flow transfers according to $\delta x(t) = \frac{dx(t)}{dt} \delta t$ with δt time independent. The projection of any displacement δx on $\nabla H(x)$ is constant, i.e. $\nabla H(x(t)) \delta x(t) = \delta E$. One can say that phase space is neither streched nor compressed in the direction along the flow and perpendicular to it. We get the equation of motion for the monodromy matrix directly, performing the following transformation that gives us a local coordinate system on the orbit $x(t)$:

$$\tilde{\mathbf{J}}(x(t)) = \mathbf{U}^{-1}(x(t)) \mathbf{J}(x(t)) \mathbf{U}(x(0)) \tag{20}$$

From this follows, using the definition of $\mathbf{L}(t)$ and the obvious fact that $\dot{\mathbf{U}}\mathbf{U}^{-1} = \mathbf{U}\dot{\mathbf{U}}^{-1}$

$$\dot{\tilde{\mathbf{J}}} = \tilde{\mathbf{L}} \tilde{\mathbf{J}} \qquad \text{with} \quad \tilde{\mathbf{L}} = \mathbf{U}^{-1}(\mathbf{L}\mathbf{U} - \dot{\mathbf{U}}) \tag{21}$$

Choosing $x_E = \nabla H(t) / |\nabla H(t)|^2$ and $x_t = \frac{dx}{dt}$ as local coordinates will give the two trivial eigenvalues 1 of the transformed matrix (20) at any time t. Setting

$$\mathbf{U} = (x_t^T, x_1^T, x_E^T, x_2^T) = \begin{pmatrix} \dot{Q}_1 & -\dot{Q}_2 & -\dot{P}_1/q^2 & -\dot{P}_2/q^2 \\ \dot{Q}_2 & \dot{Q}_1 & -\dot{P}_2/q^2 & \dot{P}_1/q^2 \\ \dot{P}_1 & \dot{P}_1 & \dot{Q}_1/q^2 & -\dot{Q}_2/q^2 \\ \dot{P}_2 & -\dot{P}_2 & \dot{Q}_2/q^2 & \dot{Q}_1/q^2 \end{pmatrix}$$

with $x = (Q_1, Q_2, P_1, P_2)^T$ and $q = |\nabla H|$, we get

$$\tilde{\mathbf{J}} = \begin{pmatrix} 1 & * & * & * \\ 0 & 1 & 0 & 0 \\ 0 & * & m_1 & m_2 \\ 0 & * & m_3 & m_4 \end{pmatrix} \qquad \tilde{\mathbf{L}} = \begin{pmatrix} 0 & * & * & * \\ 0 & 0 & 0 & 0 \\ 0 & * & l_1 & l_2 \\ 0 & * & l_3 & l_4 \end{pmatrix}$$

where

$$\mathbf{m} = \begin{pmatrix} m_1 & m_2 \\ m_3 & m_4 \end{pmatrix} \qquad \mathbf{l} = \begin{pmatrix} l_1 & l_2 \\ l_3 & l_4 \end{pmatrix}$$

$\mathbf{m}$ is the Monodromy matrix and *'s denote unknown elements. We now have the desired equation of motion for the Monodromy matrix: $\dot{\mathbf{m}} = \mathbf{lm}$ The entries in $\mathbf{l}$ can be computed from (21). Denoting partial differentiation by a footnote and setting $q = |\nabla H|^2$, they are given by:

$$\begin{aligned}
l_1 &= \frac{1}{q}[(h_{Q_1}^2 - h_{Q_2}^2 - h_{P_1}^2 + h_{p_2}^2)(h_{Q_1P_1} - h_{Q_2P_2}) \\
&\quad +2(h_{Q_1}h_{Q_2} - h_{P_1}h_{P_2})(h_{Q_1P_2} + h_{Q_2P_2}) \\
&\quad -(h_{Q_1}h_{P_1} + h_{Q_2}h_{P_2})(h_{Q_1Q_1} + h_{Q_2Q_2} - h_{P_1P_1} - h_{P_2P_2})] \\
l_2 &= \frac{1}{q^2}[(h_{Q_1}^2 + h_{P_2}^2)(h_{Q_2Q_2} + h_{P_1P_1}) + (h_{Q_2}^2 + h_{P_1}^2)(h_{Q_1Q_1} + h_{P_2P_2}) \\
&\quad -2(h_{Q_1}h_{P_1} + h_{Q_2}h_{P_2})(h_{Q_1P_1} + h_{Q_2P_2}) \\
&\quad -2(h_{Q_1}h_{Q_2} - h_{P_1}h_{P_2})(h_{Q_1Q_2} - h_{P_1P_2})] \\
l_3 &= -(h_{Q_1}^2 + h_{Q_2}^2)(h_{P_1P_1} + h_{P_2P_2}) - (h_{P_1}^2 + h_{P_2}^2)(h_{Q_1Q_1} + h_{Q_2Q_2}) \\
&\quad +2(h_{Q_1}h_{P_1} - h_{Q_2}h_{P_2})(h_{Q_1P_1} - h_{Q_2P_2}) \\
&\quad +2(h_{Q_1}h_{P_2} + h_{Q_2}h_{P_1})(h_{Q_1P_2} + h_{Q_2P_1}) \\
l_4 &= -l_1
\end{aligned}$$

Using the above equations we can integrate $\mathbf{m}$ along the cycle and then calculate the eigenvalues by

$$\Lambda = \frac{\mathrm{Tr}(\mathbf{m}) \pm \sqrt{\mathrm{Tr}(\mathbf{m})^2 - 4}}{2} \tag{22}$$

It is of course essential, that the transformation (20) of coordinates has the special form of change of basis, leaving the eigenvalues unchanged. Otherwise, the eigenvalues of $\mathbf{J}$ and $\mathbf{m}$ would not be the same and the transformation would be of no value to us. The following nomenclature is

commonly used. A cycle is called *hyperbolic* if $\Lambda = e^{\pm\lambda}$. It is called *inverse hyperbolic* if $\Lambda = -e^{\pm\lambda}$. λ/T_p is called the *Lyapunov exponent* or *stability index* of the cycle. This definition covers only real eigenvalues. For the s-wave system, this will suffice, since all eigenvalues are real. The interesting one of the two eigenvalues is the one with the largest absolute value, since this is the one that will determine how fast some little pertubation will grow. In the following we shall refer to the λ/T_p-value only for this eigenvalue as the Lyapunov exponent.

3.3 Table of cycle properties

Having explained how we determine the cycles and the properties that are interesting to us, we present in figure 4 a table containing these properties, compared to values copied from [6]. In the rest of this section, we shall comment on this table.

Regarding the action, we see that for the short cycles, the numbers match on four or five decimals, while for some of the longer cycles, the deviations appear already on the third or even second decimal. The reason for this is simply that we have not used sufficiently small timesteps in the numerical integration of the flow. We are confident that this is the only reason, since for a few cycles, e.g. $'+++++-'$ and $'+-+---'$ when decreasing the time step, the action converged towards the value given in [6]. Our excuse is that we have done all calculations on PC's, giving vast computation time for small time steps.
Regarding the Lyapunov exponents, we see that rather large deviations are present. It is interesting that these deviations do not follow the deviations in the action. Even for the cycles where the action matches precisely the action of [6], the Lyapunov exponents are clearly different. We stress again the fact that we are not using the same equations of motion as in [6]. The Kustaanheimo-Stiefel transformation introduced originally by G. Tanner and D. Wintgen for colinear Helium seems to apply both models equally well, in the sense that the calculations are effectively the same. We have used almost the same program code for the two systems, yielding actions and Lyapunov numbers for the colinear model that match very well with published results. Therefore, one can say that we have an independent check that we are doing things the right way.

4 Using the cycles

At this point, we have done the necessary determination of cycles and found the properties we need to apply the Gutzwiller Zeta function. This Zeta function is approximated using a *cycle expansion* with the cycles we have found, i.e. all cycles op to code length 6, except the '0'-cycle. Zeroes for the Zeta function are found using contour plot of the norm of the Zeta

Code	$Sp/2\pi$	Lyap.	Lyap. [6]	S_p [6]	α_p
$-$	1.72558	0.1906	0.204	1.72558	2
$+-$	3.41659	0.1943	0.183	3.41659	4
$++-$	5.06032	0.1837	0.173	5.06031	6
$+--$	5.12476	0.1864	0.171	5.12471	6
$+++-$	6.66529	0.1678	0.165	6.66529	8
$++--$	6.74245	0.1736	0.154	6.74248	8
$+---$	6.85718	0.1910	0.193	6.85734	8
$++++-$	8.24257	0.1526	0.152	8.24257	10
$+++--$	8.32641	0.1600	0.139	8.32642	10
$++-+-$	8.47268	0.1878	0.177	8.47179	10
$++---$	8.48608	0.1852	0.187	8.48562	10
$+-+--$	8.54593	0.1905	0.181	8.54751	10
$+----$	8.58112	0.1901	0.191	8.58079	10
$+++++-$	9.79987	0.1395	0.142	9.79987	12
$++++--$	9.88764	0.1476	0.126	9.88772	12
$+++-+-$	10.06914	0.1774	0.167	10.06935	12
$+++---$	10.08298	0.1756	0.179	10.07852	12
$++-+--$	10.17532	0.1847	0.174	10.17540	12
$++--+-$	10.17550	0.1843	0.174	10.17540	12
$++----$	10.20446	0.1840	0.182	10.20616	12
$+-+---$	10.27511	0.1923	0.190	10.27516	12
$+-----$	10.30755	0.1906	0.174	10.30711	12

Table 1: This table contains actions and Lyapunov exponents from our calculations (first and second column, respectively) and from [6] (fourth and third column, respectively). We have placed the columns containing the Lyapunov exponents side by side, since these are the most interesting to compare, see text.

function and a simple Newton iteration. The resulting energy spectrum is presented.

4.1 The Zeta function

What we would ideally like to do is to determine the zeroes of the *quantum spectral determinant* [5]

$$\det(E - \hat{H}) = (\text{prefactor}) \prod_n (E - E_n)$$

The zeroes determine the eigenstates E_n of the Hamilton operator $\hat{H}$. The derivation of the Gutzwiller-Voros zeta function represents a semi-classical path to an approximation of the energy spectrum. The derivation will be skipped completely here. We present only the formula itself [5]:

$$Z_{qm} = \prod_p \exp\left[-\sum_{l=1}^{\infty} \frac{\exp[l(\frac{i}{\hbar} S_p(E) - i\alpha_p \frac{\pi}{2}]}{l \left| \det(\mathbf{1} - \mathbf{J}_p^l) \right|^{(1/2)}} \right]$$

where $\mathbf{J}$ denotes the monodromy matrix, and α_p is the Morse index along the trajectory. The Morse index equals twice the code length of the cycle p. For the s-wave system, we now write the denominator as [5]:

$$|\det(\mathbf{1} - \mathbf{J})|^{-1/2} = \sqrt{|1 - \Lambda|\,|1 - \Lambda^{-1}|} = \sum_{m=0}^{\infty} |\Lambda|^{l(m+1/2)}$$

Inserting this, the sum over l in the Zeta function above gives just the expansion of a logarithm and we get the semiclassical spectral determinant as a product over dynamical zeta functions in the form

$$Z_{qm}(E) = \prod_{m=0}^{\infty} \zeta_m^{-1} = \prod_{m=0}^{\infty} \prod_p (1 - t_p^m) \tag{23}$$

where the weights t_p of each cycle is given by [6]

$$t_p^m = (\pm 1)^m \exp\left[i \left(2\pi z S_p - \alpha_p \frac{\pi}{2} \right) - \frac{1}{2} \left(m + \frac{1}{2} \right) \lambda_p S_p \right]$$

The m quantum number represents exitations that are not covered well by the s-wave model. We therefore restrict the product to m=0. Moreover, we shall consider the cycles in the *fundamental domain* instead of in the entire phase space in order to exploit the symmetry of exchanging the electrons. The fundamental domain can be visualized in the (Q_1^2, Q_2^2)-plane as the area enclosed by e.g. the Q_1^2-axis, the diagonal, and the equipotential line, see figure 3. This gives a natural splitting af the cycles into two groups: The ones that are symmetric with respect to reflection through the diagonal, and the ones that are not.

The symmetric ones will have a full phase space t_p equal to the square of the fundamental domain t_p. The ones that are not symmetric will have the same t_p in both cases, but instead, each of them will have a 'partner', namely its reflection through the diagonal. These will both contribute a factor $(1 - t_p)$. This makes us write the Zeta function as

$$\zeta_m^{-1} = \prod_{p,o}^{\infty}(1 - t_p)^2 \prod_{p,s}^{\infty}(1 - t_p^2) \tag{24}$$

Using now the simple identity $(1 + t_p)(1 - t_p) = (1 - t_p^2)$, we can factorize the above Zeta function as

$$\zeta_m^{-1} = \zeta_{m,+}^{-1}\zeta_{m,-}^{-1} \tag{25}$$

$$\zeta_{m,+}^{-1} = \prod_{p,o}^{\infty}(1 - t_p) \prod_{p,s}^{\infty}(1 - t_p) \tag{26}$$

$$\zeta_{m,-}^{-1} = \prod_{p,o}^{\infty}(1 - t_p) \prod_{p,s}^{\infty}(1 + t_p) \tag{27}$$

4.2 Cycle expansion

We now present the cycle expansion approximation to (26), using all cycles of code length up to 6, except the '0'-cycle, which we leave out. We shall write it up as suggested in [5], as a sum of the dominant *fundamental* contributions and the decreasing *curvature* terms, which are in sharp brackets:

$$\zeta^{-1} = \quad 1 \quad -t_1 - [t_{01}] - [t_{001} + (t_{011} - t_{01}t_1)] \tag{28}$$

$$\quad - \quad [t_{0001} + (t_{0111} - t_{011}t_1) + (t_{0011} - t_{001}t_1)] - ... \tag{29}$$

It is from this formula (written up to code length 6) that we determine the value of the zeta function.

4.3 Zeroes for the Zeta function

Using a contour plot of the absolute value of the zeta function, we can scan visually the complex plane, looking for zeroes. A contour plot is shown in figure 5. A systematic scan is done by the computer, using simply a Newton iteration on a large amount of points close to the real axis (as mentioned in [5] we are only looking for zeros close to the real axis) and determining whether there is convergence or not. This method appears to find all the zeroes.

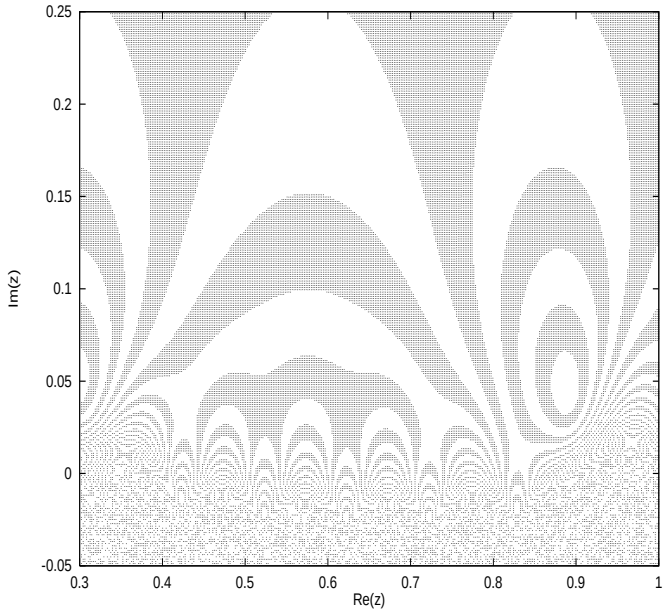

Figure 4: A contour plot of the absolute value of the zeta function. As a ground rule, circular shapes indicate a zero, but one must be carefull not to judge to soon, especially in regions where the Zeta function shows rapid variation. For the big circular spot in the right part of the plot there is no doubt, but how about the small ones that lie closer to the real axis? The front page shows a zoom in the above plot, containing clearly some zeros that could not really be seen in the above plot.

4.4 The energy spectrum

A point z, at which the Zeta function is zero, corresponds to an energy through $z = \frac{1}{\sqrt{-E}}$, see (3). In this way, we compute an energy spectrum for s-wave Helium. The results are presented in figure 6, along with energies copied from [6], where the same cycle expansion was used. Also presented are energies determined by quantum mechanical calculations, also copied from [6]. First of all, it appears that our cycle expansion yields energies very close to the energies E[6], which confirms that our computations are ok. However, we have some bad news as well. Along with all the correct zeros, the computer finds a lot of 'false' zeros.

False zeros can be a real threat to the entire method used to determine the energy spectrum, since for increasing number of false zeros, one can of course allways find zeros that lie close to any desired spectrum. Fortunately, it is not nearly that bad in our case. The computer typically finds about equally many false and real zeros. There is no trouble picking out the real ones.

We know from trying it out that when more cycles are used in the cycle expansion, the number of zeros increase. One can speculate what will happen to the problem of false zeros. It could be that the false zeros would somehow move away from the real axis when the number of cycles goes to infinity. We tried to check this by watching the zeros as we added

Config.	E	E [6]	QM
1s1s	2.587	2.581	2.879
2s2s	0.774	0.774	0.723
2s3s	0.560	0.565	0.572
3s3s	0.327	0.328	0.321
3s4s	0.263	0.265	0.265
4s4s	0.179	0.180	0.181
4s5s	0.152	0.153	0.154
4s6s	0.143	0.144	0.144
4s7s	0.137	0.136	0.138
5s5s	0.114	0.114	0.116
5s6s	0.099	0.100	0.100
5s7s	0.0959	0.0958	0.0941
5s8s	-	0.0908	0.0903

Table 2: This table gives the binding energies for the listed configurations. The first column contains the energies that we have found using our cycle expansion. The second and third column are copied from [6]. The second is found using the same cycle expansion that we have used, the third comes from quantum mechanics.

more cycles to the cycle expansion, but being limited by only cycles up to code length 6, we were unable to detect any clear effect. The problem of false zeros is also mentioned in [6].

From the table we also see that the cycle expansion gives a reasonably good prediction for the ground state binding energy, and surprisingly good predictions of many of the other states listed in the table. One must remember how simple the s-wave model is.

For some reason we cannot find the last energy in the list. We have not yet been able to find out why.

5 Conclusion

We have found all cycles up to code length 6, and made sure that given a faster computer, we could have determined the actions in exact accordance with [6].

We believe that our Lyapunov exponents are correct, although they do not match the ones in [6].

Using a cycle expansion of the Zeta function, we have calculated an energy spectrum that is in very good accordance with [6]. It may be concluded from this that the difference between our Lyapunov exponents and the ones in [6] gives only a small change in the energy spectrum.

6 An open problem

Let us consider again (5) and (6). In each of the two regions $r_1 < r_2$ and $r_1 > r_2$, the problem can be separated into

$$H_1 = E_1 = \frac{p_1^2}{2} - \frac{Z}{r_1} \qquad H_2 = E_2 = \frac{p_2^2}{2} - \frac{Z-1}{r_2} \qquad r_1 < r_2 \quad (30)$$

$$H_1 = E_1 = \frac{p_1^2}{2} - \frac{Z-1}{r_1} \qquad H_2 = E_2 = \frac{p_2^2}{2} - \frac{Z}{r_2} \qquad r_1 > r_2 \quad (31)$$

These equations describe Kepler motion in one dimension. One is tempted by this to construct a map, determining analytically the trajectory binary string given by some initial condition in the Poincaré plane.

We have unsuccessfully attempted to construct such a map. We leave this as an open problem, since time does not allow us to persue this issue further.

7 References

[1] Kai T. Hansen, Alternative method to find orbits in chaotic systems, preprint.
[2] M Draeger *et al*, Classical dynamics of s-wave Helium, Physica A 197 (1993), 113-129
[3] Klaus Richter, Semiklasik von Zwei-elektronen-atomen, Phd thesis, Freiburg, 1991
[4] Discussion with G. Tanner and P. Cvitanović
[5] P. Cvitanović and G. Tanner, Lecture notes for QC
[6] M. Draeger *et al*, One- and two-electron excitations of Helium..., Physica Review A, vol. 50, no. 5, November 1994